AD-A191 228 MICRO-RAMAN ANALYSIS OF DIELECTRIC OPTICAL THIN FILMS 1/1
(U) ROCHESTER UNIV N Y LAB FOR LASER ENERGETICS
A SCHMID 07 JAN 88 AFOSR-TR-88-0168 AFOSR-85-0221
UNCLASSIFIED F/G 7/2 NL

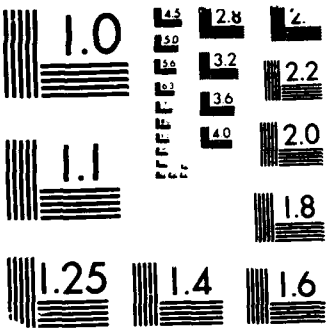

MICROCOPY RESOLUTION TEST CHART
NATIONAL BUREAU OF STANDARDS 1963-A

DTIC FILE COPY

SECURITY CLASSIFICATION OF THIS PAGE

AD-A191 228

REPORT DOCUMENTATION PAGE

1a. REPORT SECURITY CLASSIFICATION: UNCLASSIFIED	1b. RESTRICTIVE MARKINGS
2a. SECURITY CLASSIFICATION AUTHORITY	3. DISTRIBUTION / AVAILABILITY OF REPORT: Approved for public release, distribution unlimited
2b. DECLASSIFICATION / DOWNGRADING SCHEDULE	
4. PERFORMING ORGANIZATION REPORT NUMBER(S)	5. MONITORING ORGANIZATION REPORT NUMBER(S): AFOSR-TR. 88-1160
6a. NAME OF PERFORMING ORGANIZATION: Laboratory for Laser Energetics, University of Rochester; 6b. OFFICE SYMBOL (If applicable)	7a. NAME OF MONITORING ORGANIZATION: Same as 8a
6c. ADDRESS (City, State, and ZIP Code): 250 East River Road, Rochester, New York 14623	7b. ADDRESS (City, State, and ZIP Code): Same as 8b
8a. NAME OF FUNDING / SPONSORING ORGANIZATION: Air Force Office of Scientific Research; 8b. OFFICE SYMBOL (If applicable): NE	9. PROCUREMENT INSTRUMENT IDENTIFICATION NUMBER: AFOSR-85-0221
8c. ADDRESS (City, State, and ZIP Code): Building 410, Bolling Air Force Base, D.C. 20332	10. SOURCE OF FUNDING NUMBERS: PROGRAM ELEMENT NO. 61102F; PROJECT NO. 2306; TASK NO. B1; WORK UNIT ACCESSION NO.

11. TITLE (Include Security Classification)

Micro-Raman Analysis of Dielectric Optical Thin Films

12. PERSONAL AUTHOR(S)

Ansgar Schmid

13a. TYPE OF REPORT	13b. TIME COVERED	14. DATE OF REPORT (Year, Month, Day)	15. PAGE COUNT
Final Technical	FROM 05/85 TO 09/87	88-01-07	23

16. SUPPLEMENTARY NOTATION

17. COSATI CODES			18. SUBJECT TERMS (Continue on reverse if necessary and identify by block number)
FIELD	GROUP	SUB-GROUP	Zirconium oxide, Aluminum oxide, Yttrium oxide

19. ABSTRACT (Continue on reverse if necessary and identify by block number)

Wide-band-gap dielectric thin films up to 6 μm in thickness are characterized by spontaneous and stimulated Raman-gain microscopy. Materials surveyed are Al_2O_3, Y_2O_3, ZrO_2, HfO_2 and Ta_2O_5. 1-μm sized surface defects on Y_2O_3 are investigated.

20. DISTRIBUTION / AVAILABILITY OF ABSTRACT	21. ABSTRACT SECURITY CLASSIFICATION
☐ UNCLASSIFIED/UNLIMITED ☐ SAME AS RPT ☐ DTIC USERS	UNCLASSIFIED
22a. NAME OF RESPONSIBLE INDIVIDUAL: Malloy	22b. TELEPHONE (Include Area Code): (202) 767-4932
	22c. OFFICE SYMBOL: NE

DD FORM 1473, 84 MAR 83 APR edition may be used until exhausted. All other editions are obsolete.

SECURITY CLASSIFICATION OF THIS PAGE

MICRO-RAMAN ANALYSIS OF DIELECTRIC OPTICAL THIN FILMS

AFOSR - 85 - 0221

FINAL REPORT

Submitted to: Capt. K. Malloy
Air Force Office of Scientific Research

Submitted by: A. Schmid
Laboratory for Laser Energetics
University of Rochester

Contract Period: 05/01/85 through 09/30/87

Table of Contents

		Page
	SUMMARY	3
1.	INTRODUCTION	4
2.	EXPERIMENTAL SETUP	6
3.	MEASUREMENTS	9
	3.1 Spontaneous Raman Scattering Measurements	10
	3.2 Stimulated Raman Gain Measurements	12
	(A) Conventional Thin Films	12
	(B) Film Defects	13
4.	CONCLUSIONS	15
	REFERENCES	16

SUMMARY

This report describes an exploratory application of laser Raman microscopy to the characterization of defects in dielectric thin films that are UV compatible. Raman scattering provides unique vibrational information from molecular species in gaseous or condensed phases, information that can be used in identifying chemical composition, bond strength and structural conditions. Here the Raman technique is probing very small areas in model thin films. To enhance signal recovery, Raman scattering is experimentally performed in a nonlinear manner, i.e. as Raman gain spectroscopy.

1. INTRODUCTION

Laser-induced thin film damage is dominated largely by film defects. Studying their precise nature, their causes for occurrence and method of removal is subject of many investigations. A few of these investigations have used, and continue to use, spontaneous Raman scattering as a tool for characterizing defect related effects in thin films. One lengthy recent investigation[1] observed the structural changes in TiO_2 thin films in response to pulsed laser irradiation. These irradiations were carried up to the catastrophic damage threshold, and the onset of structural phase transformation of the film near damage was resolved in time. Earlier, the laser annealing[2] of TiO_2 coatings was studied by a Raman microprobe approach.

The advantage of Raman scattering to studying dielectric thin-film effects are several:

- light as a probe for structure evolution does not require the sample to be placed in vacuum as is required by charged-particle diffraction techniques;
- entirely nonionizing radiation is used;
- in multilayer structures, the design of the structures can be arranged to take full advantage of interference effects for optimizing the intensity in a specific layer of interest;[3]
- sample-grain orientation becomes measurable through the polarization relations between incident pump light and recorded Raman light;
- dielectric samples do not need to be conductively overcoated and are thus, in principle, available for other comparison studies that are similarly noncontacting, nondestructive in nature.

Raman scattering experiments on thin films are, however, not without difficulties. Scattering cross sections for dielectric compounds are small, perhaps with the exception of TiO_2 and, to a lesser extent, ThO_2, and films tend to grow amorphous on glass substrates

if no special effort is made to provide them with long-range order. The former demands care in handling the signal-to-noise issue. The latter is an intrinsic challenge because it leads to Raman peak broadening and, under truly adverse conditions, to peak disappearance.

Raman analysis of thin films is also complicated by what is called "substrate interference." This means that SiO_2 based substrates contribute substantial and broad Raman signals of their own that may mask weak Raman signals from the film. Exarhos[1] has pointed out that the contrast between these signals can be enhanced by polarization sensitive detection since glassy disorder leads to polarization anisotropy while scattering from individual randomly oriented grains is isotropic. Another approach to sidestepping this problem is use of crystalline substrates with or without distinct, easily identifiable Raman signatures. We adopted this approach on several samples here.

In this work, we have attempted applying both spontaneous and coherent Raman spectroscopies to UV-compatible thin films with special emphasis on film defect structures. The rationale for this approach was simply that little is understood about the total influence of defects on the failure modes of high-power laser coatings and that these failures become more severe the more energetic, i.e. of shorter wavelength, the laser radiation is. Since defects in state-of-the-art coatings are small, Raman microscopy had to be employed for their study.

The noncontacting, noninvasive nature of Raman microscopy made it attractive for interfacing with other optical microscopy probes that had been developed for thin-film defect analysis. One such technique is photothermal-displacement spectroscopy used in identifying absorbing defects or absorbing abnormalities in thin films. It is a particularly helpful tool in its mapping mode where its good sensitivity aids in rapidly locating absorbing defects within a film structure. Once defects are localized, they can be readily

analyzed by the more complicated and time-consuming Raman microprobe. However, defects that do not significantly absorb must be analyzed by the Raman microprobe alone.

2. EXPERIMENTAL SETUP

The main laser source for both the spontaneous and stimulated Raman experiments is a Coherent Innova I-63 Argon ion laser, operated in "light mode" for output stability. For spontaneous spectra, a prism is inserted in the cavity to enable selection of individual lines. Powers of 1-2 W are available at 514.5 nm and 488.0 nm. The beam is transported to the experimental area with a series of mirrors, the last of which form a periscope to bring the beam up to an optical rail (Newport Research Corporation MRL Series) attached perpendicular to the entrance slit of an Instruments S.A. U-1000 double monochromator. To allow visualization of the entrance slit and easy access to the optical rail, the slit cover and foreoptics are removed from the U-1000. The laser beam exiting the periscope top is perpendicular to the optical rail, and is directed along the rail away from the slit with a dichroic mirror (Omega Optical, 95% R for S-polarization @ 514.5 nm, but passing Stokes-scattered wavelengths). The excitation beam is focussed onto the sample by a high quality microscope objective (Leitz NPL, optimized for use in reflection).

The sample is kinematically mounted on a stage allowing fine positioning along the optical rail(Z) as well as in the XY plane. Z adjustment is used for focussing, with resolution of about 1 micron (Aerotech stage). X-Y positioning control is through a pair of stepper-motor driven Aerotech ATS-302 stages, with submicron resolution. The stepper motors are run by a Joerger Stepper Motor Drivers mounted in a CAMAC crate under control of a DEC LSI 11/23 microcomputer. A second Joerger unit is used to control the stepper motor grating drive in the U-1000 monochromator.

Backscattered Stokes radiation is collected by the same Leitz objective, and collimated. This scattered radiation passes through the dichroic mirror and is focussed on

the entrance slit of the monochromator by a 1" diameter f/matching lens. The U-1000 monochromator uses 1800 gr/mm holographic gratings for low ghosting and high dispersion, and has a special pair of intermediate slits which may be opened up to 1 cm. In normal operation, the intermediate slits are fully open, passing a range of wavelengths (150 wave numbers @ 514.5 nm) into the second monochromator. A special attachment in front of the exit slit of the second monochromator forms a non-vignetted image at the focal plane of a cooled EG&G PAR 1420 Intensified Linear Diode Array Detector, which is mounted above the U-1000. The detector is capable of detecting the very low levels of Stokes-scattered radiation, with amplification of about 10^5 and sensitivity of approximately 1 photo-electron. Of the 1024 elements of the array, about 700 receive an intensified signal from the standard, 18-mm intensifier, giving resolution of at least 4 pixels/wave number over the scanned region. Scattered Rayleigh light prevents collecting spectra below 180 cm^{-1} (center of array at 250 cm^{-1}). The intelligent controller for the PAR 1420 is connected to the DEC LSI 11/23 microcomputer for data storage and displays, using a National Instruments GPIB11V-1 IEEE-488 controller. Software written in FORTH is used on the LSI 11/23 to display the data on a Human Designed Systems 200G graphics terminal.

In the stimulated Raman gain (SRG) experiment, the schematic of which is shown in Fig. 1, the argon ion laser is run in all-lines mode without the intracavity prism, with total output power of approximately 4-5 W. A dichroic beam splitter (Omega Optical, 90% T @ 514.5 nm, >99% R @ 488 nm and 457.9 nm) separates the 514.5-nm line from the blue lines, which are used to pump a Coherent 599-01 Dye Laser. Coumarin 6 (Coumarin 540) dye in Benzylalcohol is used, producing at least 50 mW of power in a range from 400 cm^{-1} to 1300 cm^{-1} relative to the Argon 514.5-nm laser. These output conditions are obtained only when the dye is new, and the dye laser alignment is optimized, however. As required by the SRG experiment, the 514.5 nm beam is chopped (2.01 kHz mechanical

chopper, EG&G PAR 125A) for use as a pump beam on the sample. The dye laser output is used as the stokes beam, and is cw. Both beams are brought up to the optical rail by periscopes, and are combined on the 514.5 nm dichroic mirror. The probe (dye) beam is approximately 2 mm in diameter, and is centered on the 7-8 mm diameter pump (514.5 nm) beam. The colinear beams are focused onto the sample surface with a microscope objective, as before, and the transmitted light is collected with a 10x ESCO microscope objective and focussed on the entrance slit of the monochromator. The monochromator separates the pump from the probe beam, and passes the probe beam out the final exit slit to a UDT PIN 10D diode, operated in the photovoltaic mode with a modified UDT 101A amplifier. This diode measures the probe beam gain signal. A similar diode/amplifier combination monitors the dye-laser output power prior to the optical rail, for use as an intensity reference. The output of the signal diode is synchronously detected by an ITHACO Model 3961 Lock-In Amplifier (LIA), referenced to the chopper frequency. The output of the LIA is normalized to the reference diode level, to yield a gain signal that is independent of the dye-laser output fluctuations. The ITHACO LIA is also controlled by the GPIB interface in the LSI 11/23. Typical operating conditions for the LIA are 10-second time constant, 1-31 mV Full Scale sensitivity, Medium or High Dynamic Reserve (depending on sensitivity), bandpass input filter (Q=5), 12 dB/octave output filter. All of these settings may be changed under GPIB control. This 2.01-kHz AC detection mode justified modification of the UDT 101 A preamplifier from a broadband, low-gain to a narrow-band, high-gain device.

Searching the sample for interesting, microscopic defect features, as well as their precise location in the joint pump/probe beam focus was aided by a standard vidicon camera onto which the sample surface was imaged. This imaging capability was also used to determine whether or not, for a given sample film, the combined pump/probe intensities were excessive and caused laser damage to the coating. More important, with both pump

and probe intensities diminished by orders of magnitude, relative spatial beam overlap between pump and probe beam in the sample volume could be ascertained and maintained. Spatial overlap is critical to the success of nonlinear optics experiments such as Raman gain spectroscopy.

Raman gain curves were obtained over time periods of 30-60 minutes per peak. Long-term dye laser drifts during that time were checked by alternatingly measuring Raman gain at the lower-frequency and higher-frequency side of the peak maximum and normalizing each measurement by the instantaneous gain at the peak maximum. Since the mechanical dye-laser tuning mechanism introduces non-negligible beam wander on the sample surface, alignment adjustments were required for each data point along the gain curve. This resulted in very involved data taking.

Absolute wavelength calibration of the monochromator was carried out with the help of a miniature Neon pen lamp placed in the sample-equivalent position. The Neon discharge emission lines covered the 375 cm^{-1} to 2000 cm^{-1} wave number range on the Stokes side of the 514.5-nm Raleigh-line. For the multichannel detector, this calibration revealed a ±3 pixel peak position uncertainty after the gratings had been driven the full range. For typical solid-state Raman peak widths of several tenths of cm^{-1} this uncertainty turned out to be practically irrelevant.

3. MEASUREMENTS

Initial measurements were carried out as spontaneous Raman scattering experiments. Only after this more user-friendly method failed to yield useful data from film matrizes and defects, the nonlinear Raman gain method was employed.

3.1 Spontaneous Raman Scattering Measurements

Materials that have shown reasonable laser-damage behavior in thin-film form in the near UV were chosen as samples. With the exception of TiO_2, which we used as an instrument validation standard because it had been investigated widely before,[1] and Al_2O_3 for which prior data existed also, no Raman scattering had been reported for the most interesting compounds. These comprise Al_2O_3, Y_2O_3, HfO_2, and to a lesser extent, Ta_2O_5.

Films of different thicknesses were initially prepared by e-beam evaporation onto BK-7 glass substrates. Raman spectra were first taken from evaporant pellets in polycrystalline form. These spectra were useful in that they provided clear Raman peak position and amplitude assignments against which the spectra from films could be compared.

Invariably two phenomena were observed:

- Good spectra were obtained from crystalline imperfections, e.g., spatter grains, in thin film matrizes. These grains varied in size but were not smaller than 5 μm in diameter. The general Raman spectral features from pellets were all reproduced by the spatter-grain spectra albeit at amplitudes reduced to between 1/4 (Y_2O_3) and 1/20 (ZrO_2) of the pellet-derived spectra. As an example for this, Fig. 2 shows a $\Delta\nu = 150\ cm^{-1}$ spectral interval of the pellet (tablet) and thin-film-derived Raman spectra from Y_2O_3.
- Freshly grown films of up to 5-μm thickness were structurally disordered to the point where, without further film treatment, no useful Raman spectra could be obtained. Broad backgrounds emitted by the BK-7 substrates overwhelmed the weak film features. However, no improvement in signal-to-noise was noticed after single-crystal CaF_2 substrates were used in place of the BK-7 flats. This was true for all investigated materials, including TiO_2.

When films were sintered, sufficient order could be arranged for weak Raman spectra to be obtained. However, the elevated temperatures required for this to happen also exacerbated thermal mismatch conditions between films and substrates. Very serious film crazing and large-area decoupling between films and substrates usually occurred. Sintered, crystalline film fragments tended to yield spontaneous Raman spectra, especially from TiO_2, but at intensities inferior to those from the equivalent spatter grains. These small sample specs were largely useless for other investigations or applications.

In search of a way out of this low signal situation two issue. were briefly pursued.

- To increase film packing density, and thereby the density of scatterers per unit volume, ion-assisted film deposition was undertaken. The idea here was to transfer the momentum from several hundred eV, incident Ar ions into a forward sputtering of film constituents. Voids left unfilled by the usually columnar growth morphology of e-beam vapor-deposited films can be filled by this momentum transfer. However, at the substrate temperatures employed for this process this densification did not provide sufficient long-range order needed for improved Raman yield.
- Two samples, one a TiO_2 film the other a ZrO_2 film, were briefly analyzed by x-ray diffraction at the University of Rochester coating facility. Both samples failed to yield any Raman signals, indicative for amorphous structure conditions, while x-ray diffraction showed distinct structure rings. The issue was left unresolved because of access limitations to the diffractometer. However, the disparity clearly deserves further attention, especially for TiO_2 from which Raman spectra are quite readily obtained.

3.2 Stimulated Raman Gain Measurements

All stimulated-Raman-Gain (SRG) investigations were carried out on samples evaporated onto 2-mm thick, single-crystal CaF_2 substrates. Even under the tight focussing conditions shown in Fig. 1, where the gain length through the material is shorter than it would be in the unfocussed case, gain accumulation on broad, SiO_2-derived shoulders from the substrate had to be avoided.

(A) Conventional Thin Films

As in the case of spontaneous Raman scattering, spectra were obtained from spatter grains but not from the undisturbed film itself. This result was and remains to be counter-intuitive.

Cross sectional electronmicrographs of e-beam evaporated thin films show columnar or, as has been claimed[5], fractal growth structures. At sufficient resolution, microcrystallites ultradispersed in the amorphous columnar matrix become visible. Such ultradispersed materials have successfully been studied by Raman scattering before, first on Si[6] and later on TiO_2.[7] With the improved sensitivity afforded by the Raman-gain approach, it was hoped that Raman spectra from microcrystallites would become detectable. However, none were seen.

The dye laser tuning range employed for the gain measurement was wide enough to encompass any reasonable, or even excessive, shifts in Raman lines typically observed from ultradisperse microcrystallites. These shifts result from variation in the lattice parameters, perhaps due to internal stresses, and from the confinement-derived relaxation in wave-vector selection rules. In TiO_2, for example, microcrystals larger than 110Å exhibit anatase single-crystal Raman peak positions. Microcrystals of 55-Å average size exhibit peak shifts[7] to higher energies but of smaller magnitude the higher energetic the

original position is (12 cm^{-1}, @ 144 cm^{-1}, 2 cm^{-1} at 516 cm^{-1}). Such small shifts are well within the spectral dynamic range of our instrument.

(B) Film Defects

Analyzing film defects yielded more interesting results. Sample surfaces were searched for defect locations and defect sizes by visual inspection afforded by the video camera/monitor system. The majority of defects were spatter grains. Bulk-equivalent gain spectra were obtained from grains down to sizes at the microscope resolution limit.

Certain defects, three of which will be discussed here in greater detail, yielded spectra that were inconclusive. Figure 3 shows SEM micrographs of: the relative location of the three defects (left image) and a magnification of the top-most defect (right image). These images were obtained after completion of the Raman-gain investigation of that particular Y_2O_3 sample. Carbon overcoating was applied to the sample for the SEM work.

The moon-shaped crack in the film, visible in the left image of Fig. 3 resulted from laser damage due to excessive average power. The left-most defect produced the weakest gain signal. Signal-to-noise was improved by increasing the pump power up to the damage threshold of this particular area (1.6×10^8 W/cm^2). There is also a multitude of < 1-μm sized modular defects visible in the vicinity of the labeled defects. No gain signal was obtained from these structures.

Gain spectra from the three marked defects were identical. They resemble a 150-cm^{-1} wide peak centered at 1060 cm^{-1}. Comparison with the literature shows that a spectral feature of some peak position and about some width is obtained from Spectrosil fused quartz.[8] That spectrum is shown in Fig. 4 for two orthagonal polarizations. The gain peak from the defects located on the Y_2O_3 sample is displayed in Fig. 5 together with spatter-grain spectra obtained from either the same sample (Y_2O_2, solid line) or a ZrO_2 sample (dashed line).

The rationale for overlapping spectra as in Fig. 5 is the following: Y_2O_3 is the major impurity in ZrO_2 and vice versa. The Raman gain signal obtained form the three defects rules out that they could be crystals originating from the major impurity of the Y_2O_3 stock material. Both Y_2O_3 and ZrO_2 spectra are too different to account for the measured defect gain peak.

Further investigation shows that none of the other Raman features typical for Si-O systems are reproduced by the defect-derived spectra. A compelling identification of the defect composition from the Raman spectra alone is not possible. To resolve the contradiction, further evidence was gathered. An aerial survey by photothermal-displacement spectroscopy was hampered by the crack and related vertical displacement of the film surface and the concomittant difficulty of keeping constant focus across the mapped area. It was, however, easy to spot-check the photothermal-displacement response of individual defects and compare it with response for adjacent film patches. Since the difference in signal was insignificant, the defects could not be categorized as absorbers added to the surface perhaps by handling, transport or storage of the sample.

In a final attempt, wavelength-dispersive x-ray spectroscopy was carried out in conjunction with the SEM surface imaging. The spectral scan obtain from the defect shown individually in Fig. 3 is recorded in Fig. 6.

The incident electron energy was kept at 3 keV during the x-ray scan. For imaging purposes, a beam energy of 25 keV was chosen. The lower energy reduced the beam penetration depth and restricted the x-ray fluorescence signal to originate mostly from the defect.

The strong Y peaks at 6.21Å and 6.44Å and the absence of a Si peak at 7.21Å confirms the earlier Raman observation that the defect-related gain peak does not derive from a Si-based compound. In fact, no other low-Z element is recorded over a wider x-ray wavelength range than displayed in Fig. 5. All evidence points at Yttrium oxide as being

the composition of these defects. Yet they emit a Raman gain spectrum distinctly different from Y_2O_3 spatter grains. This implies a novel Yttrium (oxide) phase whose structure and stoichiometry we currently do not know.

4. CONCLUSIONS

Raman studies comprising spontaneous and nonlinear gain techniques were undertaken on several UV-compatible, dielectric thin films. Standard, e-beam evaporated films are structureless to the point where no Raman spectra can be obtained up to film thicknesses of several micrometers. Sintering films at elevated temperatures restores order for useful measurements, usually at a cost to the sample's structural integrity.

Although experimentally more complicated, Raman-gain measurements offer enhanced sensitivity. With the help of this technique, non-absorbing, ~1-μm sized film defects were analyzed. Defects on Y_2O_3 films, that were later identified to be made up of some stoichiometrically not defined Yttrium compound, exhibited gain spectra of unusual form. The main Raman feature, a 150-cm^{-1} wide peak, resembles both the width and peak position (1060 cm^{-1}) of a Raman signal previously recorded from SiO_2. Yet x-ray fluorescence proves that the defects contain no silicon. Unless the observed peak indicates a heretofore unknown phase of Y_2O_3, this evidence remains perplexing.

REFERENCES

1. G. J. Exarhos, "Investigate laser induced damage in optical coatings using time resolved raman spectroscopy," Report AFWL-TN-84-72.
2. L. S. Hsu, R. Solanki, G. J. Collins, and C. Y. She, Appl. Phys. Lett. 45, 1065 (1984).
3. R. J. Nemanich, C. C. Tsai, and G. N. Connell, Phys. Rev. Lett. 44, 273 (1980).
4. M. Guardalben, A. Schmid, M. Loudiana, and J. T. Dickinson, Phys. Rev. B 35, 4026 (1987).
5. R. Messier and J. E. Yehoda, J. Appl. Phys. 58, 3739 (1985).
6. G. Kanellis, J. F. Morhange, and M. Balkanski, Phys. Rev. B 21, 1543 (1980).
7. S. M. Vovk, L. M. Sharygin, and N. A. Pivavarova, J. Appl. Spectrosc. 44, 396 (1987).
8. P. F. McMillan and R. L. Remelle, Amer. Mineral. 71, 772 (1986).

FIGURE CAPTIONS

Fig. 1 Outline of the experimental setup for low-frequency modulated Raman-gain microscopy at 514.5-nm pump wavelength. Specially prepared color-separation beam splitters separate and recombine the 514.5-nm pump radiation either from Ar lines used to pump the cw dye laser or with the tunable Raman signal line ω_R. The sample rides on a X-Y stage for mapping applications. A standard video camera helps in assessing accuracy in spatial pump/signal-beam overlap on the sample surface.

Fig. 2 Comparison of spontaneous Raman spectra from Y_2O_3 polycrystalline pellet (top trace) and spatter grain (bottom trace) embedded in amorphous film matrix.

Fig. 3 Electron micrographs of micron-scale defects on Y_2O_3 thin film. Only the three labeled defects yielded a Raman-gain signal. The right micrograph is a magnification of the upper right labeled defect in the left micrograph.

Fig. 4 Raman spectrum of Si-OH and Si-O stretching modes obtained from Spectrosil fused quartz in two orthagonal polarization settings.

Fig. 5 Comparison of micro-Raman-gain spectra from defect/spatter grain structures in different thin films. Solid line represents Y_2O_3 spatter grain spectrum dashed line is spectrum from ZrO_2 grain and dot-and-dashed line displays gain peak from defects shown in Fig. 3.

Fig. 6 Wavelength-dispersive x-ray fluorescence spectrum from defect shown in right image of Fig. 3. Incident electron kinetic energy is 3 keV. Note absence of any Si signal.

Schematic Representation of Raman Gain Microscopy on Dielectric Thin Films

UR LLE

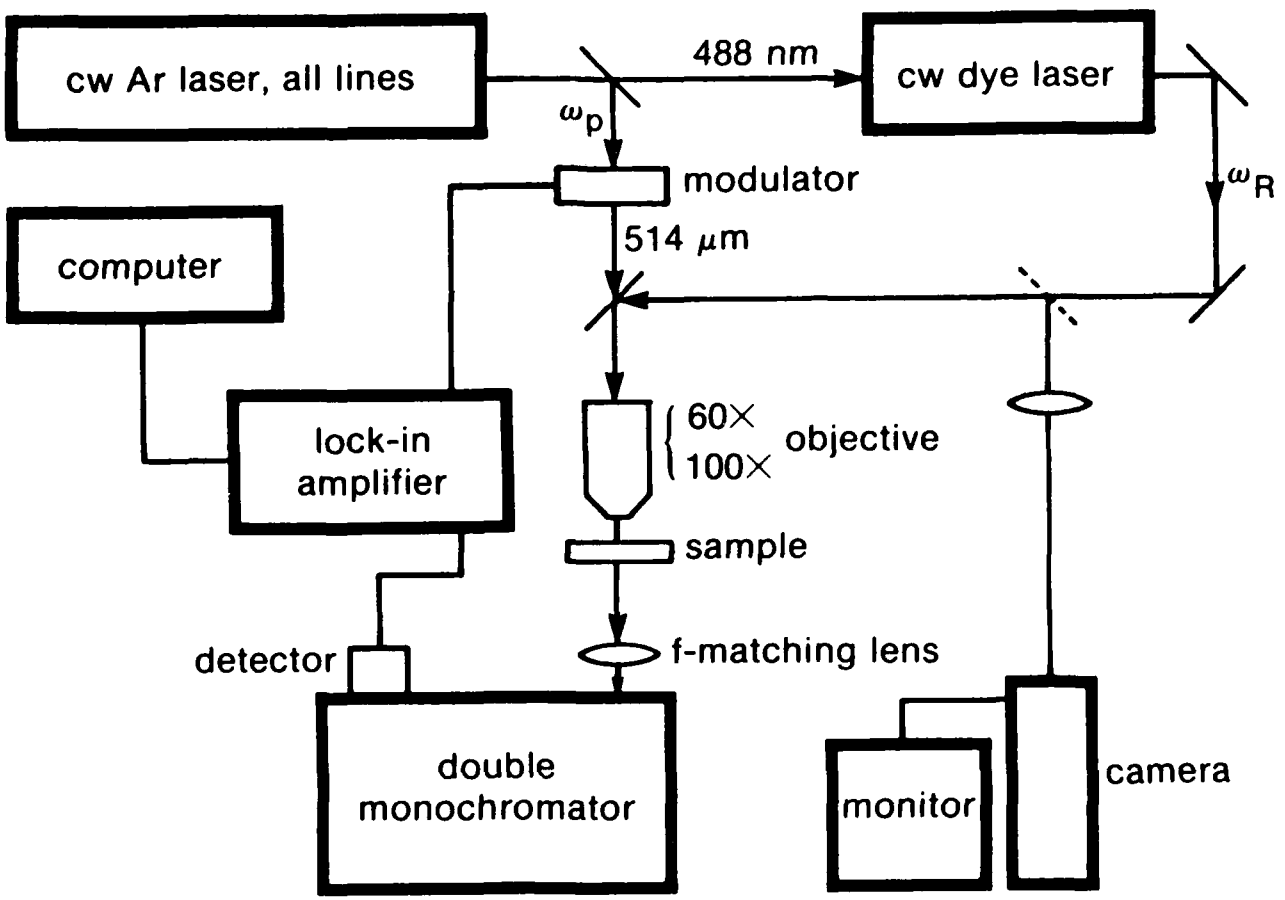

G2127

Fig. 1

Broadening and Shift of Raman Peaks in Yttria Thin Film

UR
LLE

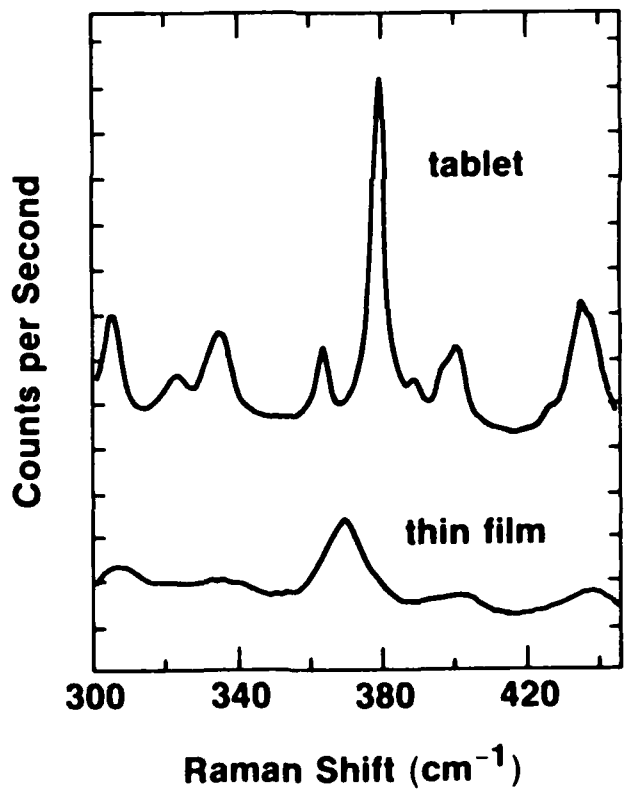

G2135

Fig. 2

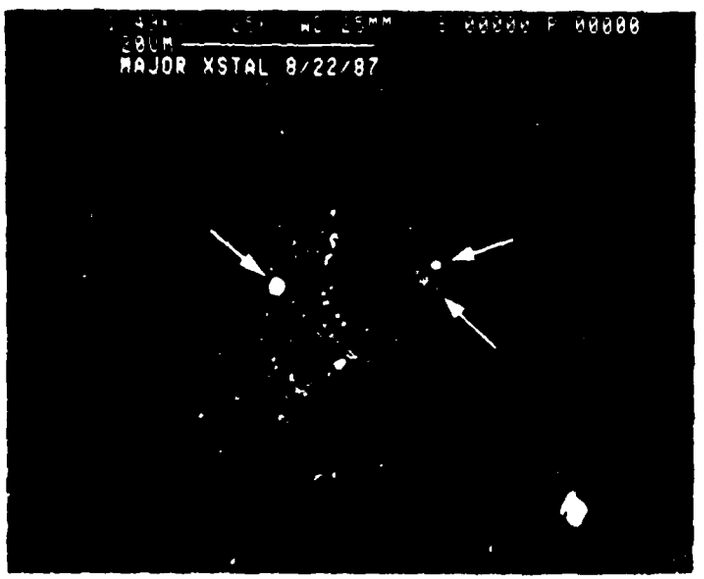

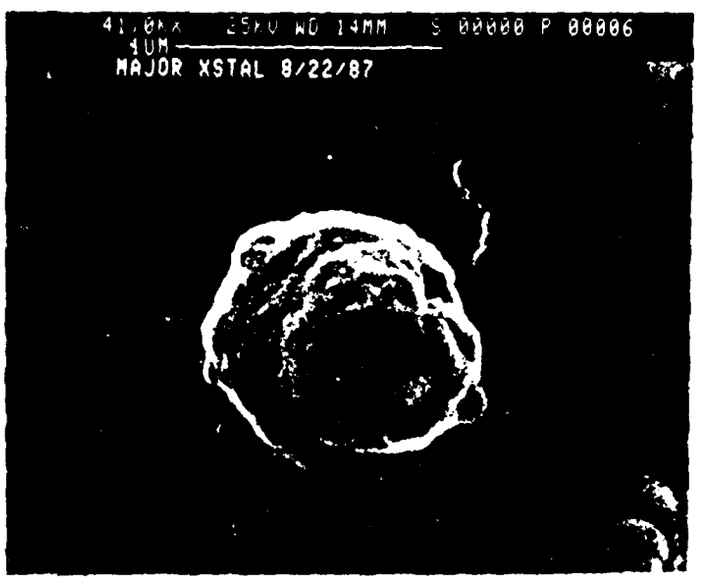

Fig. 3

Laser focal spot size: 1.5 ± 0.3 μm

- **Gain signal observed only in presence of indicated defects**

G2139

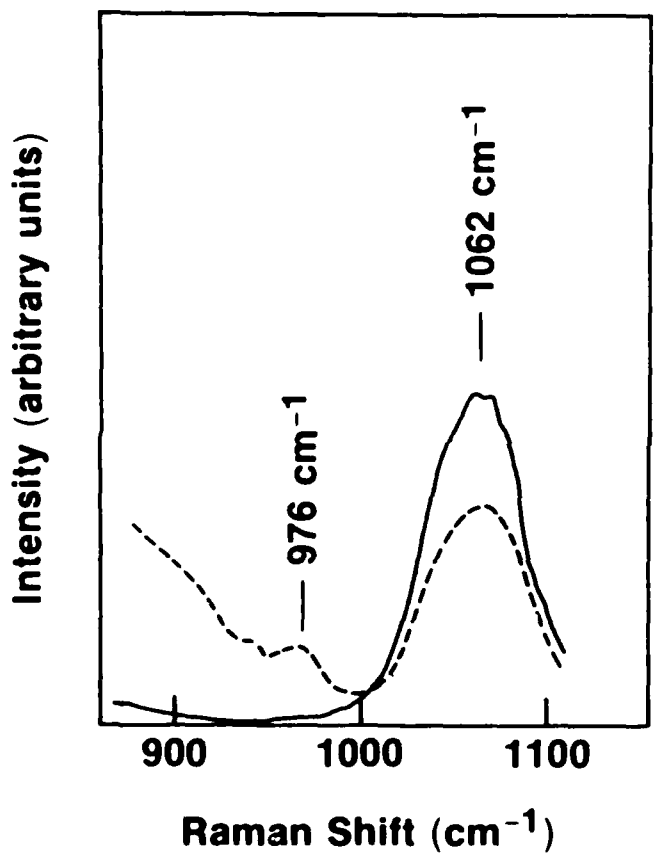

orthogonal polarizations

976 cm^{-1}: Si-OH stretching

1062 cm^{-1}: Si-O stretching

Fig. 4

From: P. F. McMillan and R. L. Remeile, Jr., *Amer. Mineral* 71, 772-778 (1986).

G2138

Unidentified Micro-Raman Gain Peak versus Standard Yttria and Zirconia Spectra

UR LLE

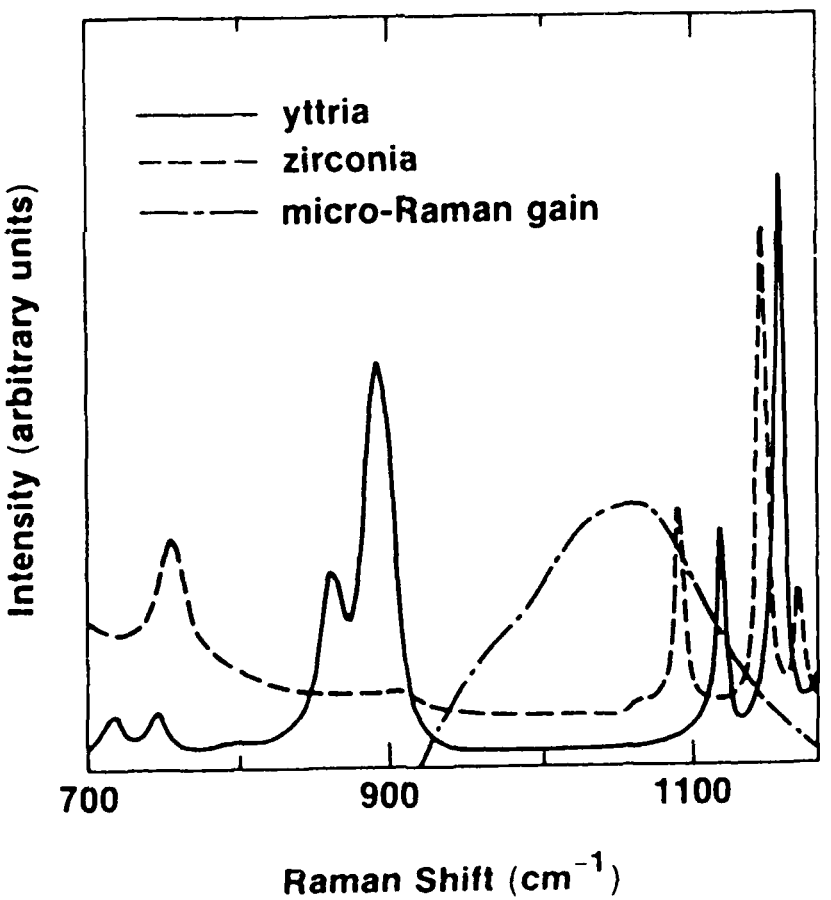

Fig. 5

G2136

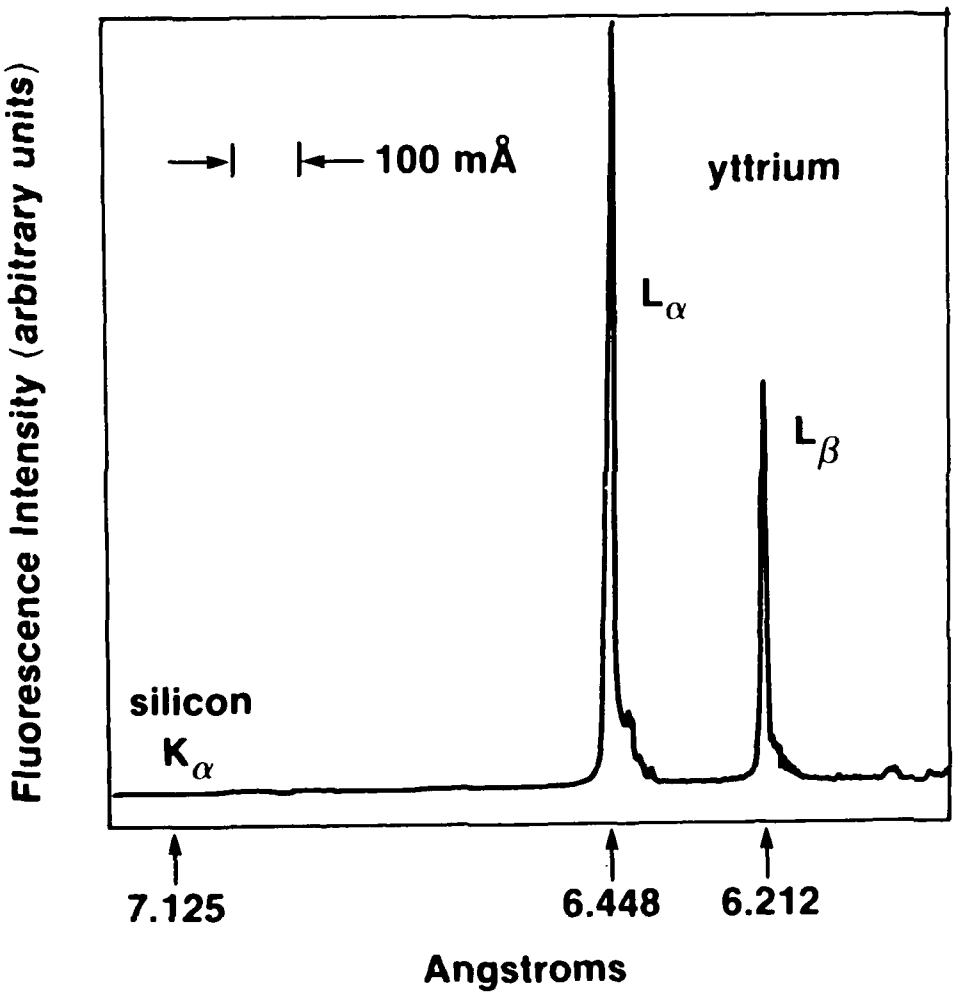
Fluorescence Intensity (arbitrary units)
100 mÅ
yttrium
L_α
L_β
silicon
K_α
7.125
6.448
6.212
Angstroms
G2137

Fig. 6

END
DATE
FILMED
5-88
DTIC